*electronics*

*Article*

# A Novel Low-Complexity Method for Near-Field Sources Based on an S-IMISC Array Model

**Xiaolin Li *, Hongjuan Yang *, Jiqu Han and Ningfei Dong**

School of Physics and Electronic Information, Yantai University, Yantai 264005, China; hanytu@163.com (J.H.); dongningfei@126.com (N.D.)
* Correspondence: lixiaolinshiwo@163.com (X.L.); yanghongjuan123.hi@163.com (H.Y.)

**Abstract:** Array optimization has recently received significant attention owing to its several advantages, such as larger array aperture and greater degrees of freedom (DOFs). However, current works focus on far-field sources, while array optimization for near-field sources has not been adequately investigated. Therefore, this work develops a new symmetry sparse array model for near-field sources based on the improved maximum inter-element spacing constraint (IMISC). The proposed symmetry IMISC (S-IMISC) array model has all the advantages of traditional sparse array models. Compared with traditional sparse array models, the S-IMISC array model affords more uniform DOFs and is less affected by mutual coupling. Additionally, in order to improve the real-time performance of near-field sources localization, the characteristic equation-based method (CEM) is used to obtain the azimuth information of near-field sources which can avoid eigenvalue decomposition (EVD), and a spectrum peak search and compression scheme is used to obtain the distance information by searching the partial area instead of the whole Fresnel area, thereby significantly reducing computation complexity. Extensive simulations verify the advantages of the proposed algorithm and the S-IMISC array model.

**Keywords:** array optimization; S-IMISC array model; near-field sources localization; CEM; compress scheme



**Citation:** Li, X.; Yang, H.; Han, J.; Dong, N. A Novel Low-Complexity Method for Near-Field Sources Based on an S-IMISC Array Model. *Electronics* **2023**, *12*, 2435. https://doi.org/10.3390/electronics12112435

Academic Editors: Yangyang Dong, Hua Chen and Fangqing Wen

Received: 25 April 2023
Revised: 23 May 2023
Accepted: 24 May 2023
Published: 27 May 2023



## 1. Introduction

Traditional wireless communication considers the user's distance to the base station to be significantly different from the antenna size of the base station. Therefore, a typical array reception model relies on the far-field assumption [1–3], i.e., the user-transmitted signal incident to the base station antenna can be regarded as a plane wave. However, in next-generation wireless communication systems, enhancing the spatial resolution of the base station and improving the spatial service ability is one of the main problems facing the current ground observation system. Currently, the ultra-large aperture antenna array model involves an aperture size ranging from several meters to tens of meters, with the near-field area extending to several kilometers. However, utilizing the traditional far-field signal model in such antennas will lead to large errors. Therefore, it is necessary to conduct in-depth theoretical and experimental research for near-field sources.

When the user is in the base station antenna array's Fresnel region, the received signal by the base station is a spherical wave. Moreover, the user's location information is determined by the azimuth and the distance between the base station and the user. Therefore, in the near-field location, it is necessary to measure the two dimensions of the target, that is, to obtain the azimuth measurement and distance measurement of the target. Nevertheless, in order to solve the problem of complex guidance vector in the near-field source model, a spherical waveform modeling based on quadratic Taylor expansion is proposed.

Based on the Simplified Near-Field Source Model, researchers have proposed several near-field positioning methods [4–7] based on a uniform linear array (ULA) model, such as the polynomial rooting method [8], Two-Stage MUSIC (TSMUSIC) [9], a gridless one-step method [10], and so on. These methods are traditional subspace methods that simultaneously realize the location of the mixed sources. Although these methods inherit the advantages of the subspace methods' high accuracy, they lose the array aperture, impose a high computational complexity, and are easily affected by the mutual coupling effect. Additionally, Chen et al. [11] suggest a maximum likelihood estimation algorithm to estimate near-field signal parameters, and Li et al. [12,13] use the idea of Sparse Signal Reconstruction to estimate near-field source parameters. Zhi et al. [14] divide the symmetric array into two sub-arrays and use their symmetry relationship to construct spectral functions for parameter estimation. The above algorithms are derived from a uniform linear array, where the number of sources is no more than 1/2 of the array elements, forcing it to lose the array's degree of freedom. Nevertheless, most algorithms require EVD and spectral peak search, resulting in high computational complexity, which increases as the array elements increase.

Several array models have been proposed to improve the array utilization, such as the nested array model [15], improved nested array model [16–19], and coprime [20–23]. These array models improve the array's degrees of freedom to a certain extent, but when the mutual coupling effect between the array elements is severe, the performance of these array models will sharply decline. Specifically, the maximum inter-element spacing constraint (MISC) array model [24] affords a good balance between mutual coupling and uDOFs. Therefore, Shi et al. [25] proposed an IMSIC array model based on MISC that outperforms the traditional MISC. It should be noted that the above improved array models are designed for far-field sources and have been poorly optimized for near-field sources. Indeed, Wang et al. [26] applied the nested array model for mixed-signal parameter estimation. Zheng et al. [27] and Su et al. [28] proposed a symmetric double nested array model (SDNA) for mixed-signal parameter estimation. Wang et al. [29] proposed an enhanced symmetric nested array model (ESNA) for mixed-signal parameters. Wang et al. [30,31] proposed a novel symmetric flipped nested array (SFNA) and an improved symmetric flipped nested array (ISFNA) for mixed-signal parameter estimation. The above im-proved nested array models can achieve higher DOF. However, these improved nested array models involve a group of uniform linear arrays, and therefore, they are affected by the mutual coupling effect, sharply degrading the positioning accuracy. Meanwhile, the above algorithms require two-dimensional search to obtain azimuth and distance information of near-field sources, which leads to high computational complexity and is not conducive to real-time performance.

Spurred by the abovementioned deficiencies, this paper introduces the S-IMISC array model based on IMSIC. The S-MISC array model has all the advantages of the nested array models. In the case of a certain number of arrays, the positioning of the S-IMISC array can be uniquely determined by a closed formula. However, compared with nested array models, the S-IMISC array model has more degrees of freedom and reduces the influence of the mutual coupling effect. Extensive experimental simulation results reveal that the proposed algorithm has advantages over the existing sparse algorithms in an array configuration. The S-IMISC array model is not only suitable for near-field source localization but also applies mixed-source localization.

Meanwhile, to reduce our algorithm's computational complexity and improve its real-time performance, we utilize the CEM algorithm [32] to estimate the azimuth of near-field sources and thus avoid the EVD process and the spectral peak search. Furthermore, the compressed MUSIC algorithm [33] is incorporated into the distance parameter estimation. The distance search area is divided into distance slices to construct a group of noise subspace clusters and their intersection is calculated. The spectral function is constructed using the newly constructed intersection, which transforms the original Fresnel region search into a small region search, further reducing our algorithm's computational complexity and processing time.

The rest of the paper consists of six sections. The novel array model and the near-field source model are briefly reviewed in Section 2. The proposed algorithm of the azimuth estimation for near-field sources is introduced in Section 3. The proposed algorithm of range estimation for near-field sources is introduced in Section 4. The performance analysis of the S-MISC array model and the proposed algorithm will be presented in Section 5. In Section 6, we will use some numerical examples to verify the effectiveness of the S-MISC array model and the proposed algorithm in this paper. The paper will be concluded in Section 7. Compared with the existing algorithms and sparse array models, the special array model structure provides the two important advantages, namely: larger aperture and a smaller effect of mutual coupling. Combining the use of CEM algorithm ideas and compression scheme allows to reduce computational complexity and improve real-time performance. The above two major advantages make the proposed algorithm and the S-IMISC array model very suitable for near-field source localization.

## 2. Array Model and Signal Model of the Near-Field Source

### *2.1. S-IMISC Array Model*

Next, we introduce the S-IMISC array model, which comprises 12 sparse ULAs and consists of $2N-1$ array elements. The S-IMISC array model has more desirable properties and advantages than nested and coprime arrays, such as a lower mutual coupling effect and more DOFs. We define $M$ as the maximum array element spacing and $\mathbb{D}$ as distance between adjacent elements. The S-IMISC array model is an array symmetrical with central elements, where $\mathbb{D}_{S-IMISC-F}$ is the distance between adjacent elements which is located on the right side of the central array element and $\mathbb{D}_{S-IMISC-D}$ is the distance between adjacent elements which is located on the left side of the central array element. Then, $M$ and $\mathbb{D}$ are used to locate the S-IMISC array model, as follows:

$$M = 4\left\lfloor \frac{N+2}{6} \right\rfloor N \geq 10, \tag{1}$$

$$\mathbb{D} = [\mathbb{D}_{S-IMISC-D}\ \mathbb{D}_{S-IMISC-F}], \tag{2}$$

$$\mathbb{D}_{S-IMISC-F} = \left[ \underbrace{2,\ldots,2}_{\frac{M}{4}-1}, 1, 1, \frac{M}{2}-2, \underbrace{\left(\frac{M}{2}-1\right),\ldots,\left(\frac{M}{2}-1\right)}_{\frac{M-4}{2}}, \underbrace{M,\ldots,M}_{N-M}, \left(\frac{M}{2}+1\right), \underbrace{\left(\frac{M}{2}+1\right),\ldots,\left(\frac{M}{2}+1\right)}_{\frac{M-4}{2}}, 2, \underbrace{2,\ldots,2}_{\frac{M-4}{2}} \right], \tag{3}$$

$$\mathbb{D}_{S-IMISC-D} = \left[ \underbrace{2,\ldots,2}_{\frac{M-4}{2}}, 2, \underbrace{\left(\frac{M}{2}+1\right),\ldots,\left(\frac{M}{2}+1\right)}_{\frac{M-4}{2}}, \left(\frac{M}{2}+1\right), \underbrace{M,\ldots,M}_{N-M}, \underbrace{\left(\frac{M}{2}-1\right),\ldots,\left(\frac{M}{2}-1\right)}_{\frac{M-4}{2}}, \frac{M}{2}-2, 1, 1, \underbrace{2,\ldots,2}_{\frac{M}{4}-2} \right]. \tag{4}$$

The position $\mathbb{P}$ of the array element corresponding to Formula (2) is as follows:

$$\mathbb{P} = [\mathbb{P}_{S-IMISC-D} \quad \mathbb{P}_{S-IMSIC-F}] = [p_{-N+1}, \ldots, p_{N-1}] \tag{5}$$

$$\mathbb{P}_{S-IMISC-D} = \left\{ \begin{array}{l} \underbrace{-\left(MN - \frac{3M^2}{4} - 1\right), \ldots, -\left(MN - \frac{3M^2}{4} - \frac{M}{2} + 1\right)}_{ULA12, IES=2} \\ \underbrace{-\left(MN - \frac{3M^2}{4} - \frac{M}{2} - 1\right), \ldots, -\left(MN - \frac{7M^2}{8} - \frac{M}{4} + 1\right)}_{ULA11, IES=\frac{M}{2}+1} \\ \underbrace{-\left(MN - \frac{7M^2}{8} - \frac{M}{4}\right), \ldots, -\left(\frac{M^2}{8} + \frac{3M}{4}\right),}_{ULA10, IES=M} \\ \underbrace{-\left(\frac{M^2}{8} - \frac{M}{4}\right), \ldots, -(M-2),}_{ULA9, IES=\frac{M}{2}-1} \underbrace{-\frac{M}{2}, \ldots, -\left(\frac{M}{2} - 1\right),}_{UL8, IES=1} \underbrace{-\left(\frac{M}{2} - 2\right), \ldots, -2}_{UL7, IES=2} \end{array} \right\}, \tag{6}$$

$$\mathbb{P}_{S-IMISC-F} = \left\{ \begin{array}{l} \underbrace{0, \ldots, \frac{M}{2} - 2,}_{UL1, IES=2} \underbrace{\frac{M}{2} - 1, \frac{M}{2},}_{UL2, IES=1} \underbrace{M-2, \ldots, \frac{M^2}{8} - \frac{M}{4},}_{ULA3, IES=\frac{M}{2}-1} \\ \underbrace{\frac{M^2}{8} + \frac{3M}{4}, \ldots, MN - \frac{7M^2}{8} - \frac{M}{4},}_{ULA4, IES=M} \\ \underbrace{MN - \frac{7M^2}{8} - \frac{M}{4} + 1, \ldots, MN - \frac{3M^2}{4} - \frac{M}{2} - 1,}_{ULA5, IES=\frac{M}{2}+1} \\ \underbrace{MN - \frac{3M^2}{4} - \frac{M}{2} + 1, \ldots, MN - \frac{3M^2}{4} - 1}_{ULA6, IES=2} \end{array} \right\}. \tag{7}$$

The array positions of the S-IMISC array configuration are illustrated in Figure 1, where the location of an array can be represented as a function of $N$ and $M$. Since $M$ is determined by $N$, the S-IMISC array has a closed-form expression for the location of an array concerning an arbitrary number of arrays.

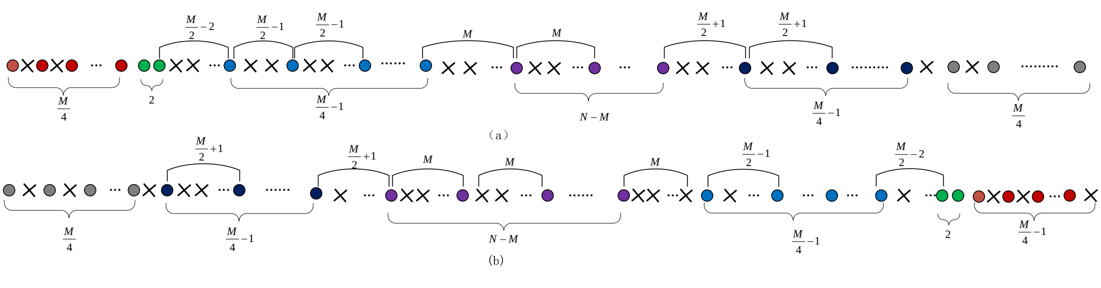


**Figure 1.** S-IMISC array model: (**a**) forward array and (**b**) backward array.

## 2.2. Signal Model of the Near-Field Sources

As depicted in Figure 1, $L$ narrowband near-field sources are irradiated on a symmetric non-uniform linear array with $2N-1$ non-directional arrays. Assuming that the center of the array is a phase reference point, the data received by array $i$ can be shown as follows:

$$x_i(t) = \sum_{k=1}^{L} a_i(\theta_k, r_k) s_k(t) + n_i(t) \quad -N+1 \leq \ i \leq N-1, \tag{8}$$

where $s_k(t)$ is the $k$th narrowband near-field source and $n_i(t)$ is the additive Gaussian noise received by the $i$th array.

The vector form of the data received by the arrays can be expressed as:

$$\boldsymbol{x}(t) = \boldsymbol{A}(\theta, r)\boldsymbol{s}(t) + \boldsymbol{n}(t), \tag{9}$$

where $\boldsymbol{s}(t) = [s_1(t), \cdots, s_L(t)]^{\mathrm{T}}$ is a $L \times 1$ vector of the near-field sources, $\boldsymbol{n}(t)$ is the $(2N-1) \times 1$ Gaussian white noise vector.

Moreover, $\boldsymbol{A}(\theta, r)$ represents the near-field source manifold matrix, expressed as:

$$\boldsymbol{A}(\theta, r) = [\boldsymbol{a}(\theta_1, r_1), \cdots, \boldsymbol{a}(\theta_L, r_L)], \tag{10}$$

$$a(\theta_k, r_k) = \left[exp(j\left(-p\omega_k + N^2\phi_k\right)\right), \ldots, \exp\left(j\left(N\omega_k + N^2\phi_k\right)\right)]^T, \tag{11}$$

where $\omega_k, \phi_k$ are:

$$\omega_k = -2\pi d \sin(\theta_k)/\lambda, \tag{12}$$

$$\phi_k = \frac{\pi d^2 \cos(\theta_k)^2}{\lambda r_k}, \tag{13}$$

where $\theta_k$ and $r_k$ $k = [1, 2, \cdots, L]$ are the azimuth and distance of the $k$th near-field source.

This paper makes the following assumptions:

(1) Near-field sources are statistically independent of each other;
(2) The sensor noise is additive Gaussian white noise and does not depend on the source;
(3) The smallest array interval is the wavelength of $1/4$.

Based on the above assumptions, we will estimate the azimuth and the distance of the near-field signal.

## 3. The Azimuth Estimation for Near-Field Sources Based on the S-IMISC Array

First, to estimate the azimuth information of the near-field source, a fourth-order cumulative vector based on the S-IMISC array model is constructed as follows:

$$\begin{aligned} C(i, -i, j, -j) &= cum\left\{x_i, x_{-i}^*, x_j^*, x_{-j}\right\} \\ &= \sum_{m=1}^{L} c_{4si} a_m(i) a_m^*(-i) a_m^*(j) a_m(-j) \\ &= \sum_{m=1}^{L} c_{4si} e^{j(2(p_i - p_j)\omega_m)}, \end{aligned} \tag{14}$$

where $c_{4si} = cum(s_m(t), s_m(t), s_m(t), s_m(t))$.

Based on the S-IMISC array model, we construct the $N-1$ positive difference as follows:

$$\begin{cases} C_1 = \{p_1 - p_0, \ldots, p_{N-1} - p_0\} \\ C_2 = \{p_2 - p_1, \ldots, p_{N-1} - p_1\} \\ C_3 = \{p_3 - p_2, \ldots, p_{N-1} - p_2\}. \\ \quad \vdots \\ C_{N-1} = \{p_{N-1} - p_{N-2}\} \end{cases} \tag{15}$$

From the integer set $D_{S-IMISC}$, the difference set of an S-MISC array is provided by a consecutive set from $[-MN + \frac{3M^2}{4} + \frac{M}{2} - 1, \ldots, MN - \frac{3M^2}{4} - \frac{M}{2} + 1]$.

$$D_{S-IMISC} = \left\{-MN + \frac{3M^2}{4} + \frac{M}{2} - 1, \ldots, -2, -1, 0, 1, 2, \ldots, MN - \frac{3M^2}{4} - \frac{M}{2} + 1\right\}, \tag{16}$$

The proof of (16) has been derived [13].

Therefore, the uniform DOFs for the S-IMISC array model is

$$uDOFs = 2MN - \frac{3M^2}{2} - M + 3. \tag{17}$$

From Formula (15), we obtain a fourth-order cumulative vector $C_{S-IMISC}$ of $2MN - \frac{3M^2}{2} - M + 3$ dimension as follows:

$$C_{S-IMISC} = \sum_{i=1}^{L} c_{4si} exp(\mathrm{j}2i\omega_i), i \in \left[-MN + \frac{3M^2}{4} + \frac{M}{2} - 1, MN - \frac{3M^2}{4} - \frac{M}{2} + 1\right]. \tag{18}$$

Traditional algorithms require EVD and spectral peak search, which increase the calculation burden. Thus, this paper utilizes the CEM algorithm to avoid EVD and spectral peak search and thus reduce calculation complexity. The specific steps are as follows:

First, we construct a polynomial of the following order:

$$f(\chi) = \prod_{k=1}^{L}\left(\chi - e^{(j2\omega_k)}\right) = \chi^L + c_{L-1}\chi^{L-1} + \cdots + c_1\chi^1 + c_0. \tag{19}$$

Formula (19) reveals the roots on the unit circle corresponding to the azimuth information of the information sources. Therefore, it is only necessary to determine the polynomial coefficients $[c_{L-1}, c_{L-2}, \cdots, c_0]$, construct Formula (19) and solve it to obtain the azimuth information of the information sources.

To facilitate derivation, we define $P = 2MN - \frac{3M^2}{2} - M + 3$. Then, we bring the solution $\mathrm{e}^{\mathrm{j}2\omega_k}$ into Formula (19) to satisfy the following:

$$e^{j2\omega_k L} + c_{L-1}e^{j2\omega_k(L-1)} + \cdots + c_1 e^{j2\omega_k} + c_0 = 0 \; k = 1, 2, \cdots, L. \tag{20}$$

After that, we multiply both sides of Formula (20) by factors to obtain Formula (21) as follows:

$$\begin{cases} c_{4s1}e^{j2\omega_1 J}e^{j2\omega_1 L} + c_{4s1}e^{j2\omega_1 J}c_{L-1}e^{j2\omega_1(L-1)} + \cdots + c_{4s1}e^{j2\omega_1 J}c_1 e^{j2\omega_1} + c_{4si}e^{j2\omega_1 J}c_0 = 0 \\ \vdots \\ c_{4sL}e^{j2\omega_L J}e^{j2\omega_L L} + c_{4sL}e^{j2\omega_L J}c_{L-1}e^{j2\omega_L(L-1)} + \cdots + c_{4sL}e^{j2\omega_L J}c_1 e^{j2\omega_L} + c_{4sL}e^{j2\omega_L J}c_0 = 0 \end{cases}, \tag{21}$$

where $J = -P, \cdots 0, \cdots, P - L$.

The following formula can be obtained by superposition of Formula (21):

$$\sum_{i=1}^{L} c_{4si}\mathrm{e}^{\mathrm{j}2\omega_i J}\mathrm{e}^{\mathrm{j}2\omega_i L} + \sum_{i=1}^{L} c_{4si}\mathrm{e}^{\mathrm{j}2\omega_i J}c_{L-1}\mathrm{e}^{\mathrm{j}2\omega_i(L-1)} + \cdots + \sum_{i=1}^{L} c_{4si}\mathrm{e}^{\mathrm{j}2\omega_i J}c_1\mathrm{e}^{\mathrm{j}2\omega_i} + \sum_{i=1}^{L} c_{4si}\mathrm{e}^{\mathrm{j}2\omega_i J}c_0 = 0 \tag{22}$$

When Formula (18) is introduced into Formula (22), Formula (22) can be rewritten as follows:

$$C(J+L) + \boldsymbol{C}(J+L-1)c_{L-1} + \cdots + \boldsymbol{C}(J+1)c_1 + \boldsymbol{C}(J)c_0 = 0 \tag{23}$$

Next, we rewrite the $2P - L + 1$ equations into a matrix as follows:

$$\begin{bmatrix} \boldsymbol{C}(-P) \;\; \boldsymbol{C}(-P+1)\cdots\boldsymbol{C}(-P+L-1) \\ \boldsymbol{C}(-P+1)\boldsymbol{C}(-P+2)\cdots\boldsymbol{C}(-P+L) \\ \vdots\vdots\ddots\vdots \\ \boldsymbol{C}(P-L)\boldsymbol{C}(P-L+1)\cdots\boldsymbol{C}(P-1) \end{bmatrix}\begin{bmatrix} c_0 \\ c_1 \\ \vdots \\ c_{L-1} \end{bmatrix} = -\begin{bmatrix} \boldsymbol{C}(-P+L) \\ \boldsymbol{C}(-P+L+1) \\ \vdots \\ \boldsymbol{C}(P) \end{bmatrix}. \tag{24}$$

Formula (24) reveals that the coefficient of the polynomial $[\bar{c}_{L-1}, \bar{c}_{L-2}, \cdots, \bar{c}_0]$ can be obtained as long as the value of $C$ is determined.

The polynomial coefficients obtained are input into Formula (19) as follows:

$$f(\chi) = \prod_{k=1}^{L} \left( \chi - e^{(j2\omega_k)} \right) = \chi^L + \overline{c_{L-1}} \chi^{L-1} + \cdots + \overline{c_1} \chi^1 + \overline{c_0}. \tag{25}$$

After obtaining Formula (25), we solve it to obtain the roots and then use Formula (26) to convert the $L$ roots to calculate the azimuth parameters of the near-field source.

$$\theta_i = \sin^{-1}(arg(\chi_k)\lambda/(4\Pi d))i = 1, 2, \cdots, L. \tag{26}$$

**4. Distance Estimation for Near-Field Sources Based on the S-MISC Array Model**

This section obtains the distance of information from near-field sources. Specifically, we construct the covariance matrix $\boldsymbol{R}$ with using the data received by the forward arrays presented in Figure 1b, as follows:

$$\boldsymbol{R} = E\left( \boldsymbol{x}(t) \boldsymbol{x}^H(t) \right) = \boldsymbol{A} \boldsymbol{R}_s \boldsymbol{A}^H + \sigma^2 I. \tag{27}$$

By applying EVD on the covariance matrix, we obtain the following:

$$\boldsymbol{R} = \boldsymbol{U} \Lambda \boldsymbol{U}^H = \boldsymbol{U}_S \boldsymbol{\Lambda}_S \boldsymbol{U}_S^H + \boldsymbol{U}_N \boldsymbol{\Lambda}_N \boldsymbol{U}_N^H, \tag{28}$$

where the signal subspace $\boldsymbol{U}_S$ is stretched by the eigenvector that corresponds to the large eigenvalue, and the noise subspace $\boldsymbol{U}_N$ is stretched by the eigenvector corresponding to the small eigenvalue.

The orthogonality principle between the signal and noise subspace is used to construct a new formula, where the distance information of the signal is obtained by minimizing the spectral Formula (29):

$$r_i = \min(\boldsymbol{a}^H(\theta_i, r) \boldsymbol{U}_N \boldsymbol{U}_N^H \boldsymbol{a}(\theta_i, r)). \tag{29}$$

Traditional algorithms generally use spectral peak search to obtain the distance information of the near-field sources. However, this strategy imposes a huge computational complexity, prohibiting real-time processing. Hence, the algorithm proposed in this paper searches only for a part of the area instead of the whole area, reducing the computational burden.

This section focuses on the simplified operation of the range spectrum peak search part. Particularly, the whole range space is divided into $\beta$ small areas for search. The division between the cells is illustrated in Figure 2.

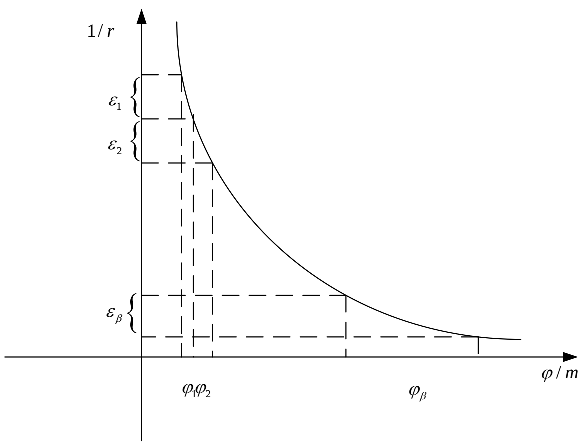


**Figure 2.** Spatial range division.

The corresponding value range is uniformly distributed, as shown below:

$$\varepsilon_1 = \varepsilon_2 = \varepsilon_3 \dots \varepsilon_\beta = \frac{k}{\beta} = \varepsilon. \tag{30}$$

Therefore, we obtain the following relationship:

$$\varphi_1 < \varphi_2 < \varphi_3 = \cdots < \varphi_\beta. \tag{31}$$

The mapping relationship between the distance intervals $\varphi_k$ and $\varphi_m$ meets the following requirements:

$$f : \varphi_k \to \varphi_m, f(r_k) = \frac{1}{r_k} + (k-m)\varepsilon \to \frac{1}{r_m}. \tag{32}$$

According to the above analysis, for any distance value $r_k$ in the distance range $\varphi_k$, there must be a distance value $r_m$ in the distance range $\varphi_m$ corresponding to $r_k$.

Assumption: $\theta_m$ is the angular information, $r_m$ is the range information concerning $\theta_m$ and $a_i(\theta, r)$ is the $i$th element of the guiding vector $\boldsymbol{a}(\theta, r)$.

By introducing Formula (32) into the guidance vector of the near-field source signal, we obtain the following:

$$\begin{aligned} a_i(\theta_m, r_m) &= exp(-j2\pi d p_i \sin(\theta_m)/\lambda + j\pi d^2 {p_i}^2 \cos(\theta_m)^2/\lambda r_m) \\ &= exp(-j2\pi d p_i \sin(\theta_m)/\lambda + j\pi d^2 {p_i}^2 \cos(\theta_m)^2/\lambda(\tfrac{1}{r_k} + (k-m)\varepsilon)) \\ &= exp(-j2\pi d p_i \sin(\theta_m)/\lambda + j\pi d^2 {p_i}^2 \cos(\theta_m)^2/\lambda r_k) \times exp(j\pi d^2 {p_i}^2 \cos(\theta_m)^2/\lambda)(k-m)\varepsilon)), \\ &= \chi_{k,i} a_i(\theta_m, r_k) \end{aligned} \tag{33}$$

where $\chi_{k,i}$ is a fixed constant, defined as follows:

$$\chi_{k,i} = exp(j\pi d^2 {p_i}^2 \cos(\theta_m)^2/\lambda)(k-m)\varepsilon)) \tag{34}$$

Therefore, $a(\theta_m, r_m)$ and $a(\theta_m, r_k)$ can be written as follows:

$$\begin{aligned} \boldsymbol{a}(\theta_m, r_m) &= [\chi_{k,-N+1} a_{-N+1}(\theta_m, r_k), \cdots, \chi_{k,0} a_0(\theta_m, r_k), \cdots, \chi_{k,N-1} a_{N-1}(\theta_m, r_k)] \\ &= [\chi_{k,-N+1}, \cdots, \chi_{k,0}, \cdots, \chi_{k,N-1}] \odot [a_{-N+1}(\theta_m, r_k), \cdots, a_0(\theta_m, r_k), \cdots, a_{N-1}(\theta_m, r_k)], \\ &= \boldsymbol{\chi}_k \odot \boldsymbol{a}(\theta_m, r_k) \end{aligned} \tag{35}$$

where $\odot$ symbolizes the Hadamard multiplication and $\boldsymbol{\chi}_k$ is a $(2N-1) \times 1$ dimensional vector defined as $\boldsymbol{\chi}_k = [\chi_{k,-N+1}, \dots, \chi_{k,0}, \dots, \chi_{k,N-1}]^{\mathrm{T}}$.

According to the principle that the guiding vector of the signal subspace is orthogonal to the noise subspace, it can be concluded that:

$$\langle a(\theta_m, r_m), u_i \rangle = 0, i = 1, 2 \cdots (2N+1-K), \tag{36}$$

where $\langle ., . \rangle$ symbolizes the Khatri–Rao (column-wise Kronecker) matrix product and $\boldsymbol{u}_i$ is the $i$th column vector of the initial noise subspace U.

By combining Formulas (35) and (36), we obtain the following:

$$\begin{aligned} \langle \boldsymbol{a}(\theta_m, r_m), \boldsymbol{u}_i \rangle &= \langle \boldsymbol{\chi}_k \odot \boldsymbol{a}(\theta_m, r_k), \boldsymbol{u}_i \rangle \\ &= \langle \boldsymbol{a}(\theta_m, r_k), \boldsymbol{\chi}_k^* \odot \boldsymbol{u}_i \rangle \\ &= \langle \boldsymbol{a}(\theta_m, r_k), \boldsymbol{u}_{i,k} \rangle = 0 \end{aligned} \tag{37}$$

where $\boldsymbol{u}_{i,k} = \chi_k^* \odot \boldsymbol{u}_i$ is the $i$th column vector of $\boldsymbol{U}_k$.

$$\begin{aligned} \boldsymbol{U}_k &= \left[\boldsymbol{u}_{1,k}, \boldsymbol{u}_{2,k}, \cdots, \boldsymbol{u}_{(2N-1-L),k}\right] \\ &= \left[\chi_k^* \odot u_1, \chi_k^* \odot u_2, \cdots, \chi_k^* \odot \boldsymbol{u}_{(2N-1-L)}\right] \\ &= \left[\underbrace{\chi_k^*, \chi_k^*, \cdots, \chi_k^*}_{(2N-1-L)}\right] \odot \left[\boldsymbol{u}_1, \boldsymbol{u}_2, \cdots, \boldsymbol{u}_{(2N-1-K)}\right]. \end{aligned} \tag{38}$$

To facilitate the following derivation, we define the original noise subspace $\boldsymbol{U}$ as:

$$\boldsymbol{U} = \boldsymbol{U}_1. \tag{39}$$

Therefore, $\boldsymbol{U}_k, k = 1, 2, \cdots, \beta$ is called the noise subspace cluster. Next, we construct the intersection $\boldsymbol{U}_{new}$ of the noise subspace clusters $\boldsymbol{U}_k, k = 1, 2, \cdots, \beta$, namely:

$$span(\boldsymbol{U}_{new}) = \bigcap_{k=1}^{\beta} \text{span}(\boldsymbol{U}_k). \tag{40}$$

Formula (39) highlights that span$(\boldsymbol{U}_{new})$ contains only partial vectors of each subspace in the noise subspace cluster. In another way, the dimension of span$(\boldsymbol{U}_{new})$ is smaller than each subspace in the noise subspace cluster, namely:

$$span(\boldsymbol{U}_{new}) \subseteq span(\boldsymbol{U}_k). \tag{41}$$

According to the above derivation, the $\boldsymbol{a}(\theta_m, r_m)$ and $\boldsymbol{U}_m$ orthogonality is equivalent to the $\boldsymbol{a}(\theta_m, r_k)$ and $\boldsymbol{U}_k$ orthogonality. Meanwhile, $\boldsymbol{U}_{new}$ is the intersection of the noise subspace cluster $\boldsymbol{U}_k, k = 1, 2, \cdots, \beta$, so $\boldsymbol{a}(\theta_m, r_k), k = 1, 2, \ldots, \beta$ is orthogonal to $\boldsymbol{U}_{new}$.

$$\boldsymbol{a}(\theta_m, r_k) \perp span(U_{new}), k = 1, 2, \ldots, \beta. \tag{42}$$

According to the orthogonality of $\boldsymbol{a}(\theta_m, r_k)$ and span$(\boldsymbol{U}_{new})$, a new spectral function of distance estimation is constructed:

$$\max_r P_{new}(r) = \frac{1}{\boldsymbol{a}^H(\theta_m, r)\hat{\boldsymbol{U}}_{new}\hat{\boldsymbol{U}}_{new}^H \boldsymbol{a}(\theta_m, r)} = \frac{1}{\left\|\hat{\boldsymbol{U}}_{new}^H \boldsymbol{a}(\theta_m, r)\right\|}. \tag{43}$$

Then, we substitute the azimuth information of the $m$-th near-field source into Formula (42) and search the whole Fresnel region to obtain the $\beta$ distance information, including a true distance $r_m$ and false distances $r_k, k = 1, 2 \ldots (\beta - 1)$. From another perspective, there is a real distance corresponding to $\beta - 1$ false distances, which is shown in Figure 3.

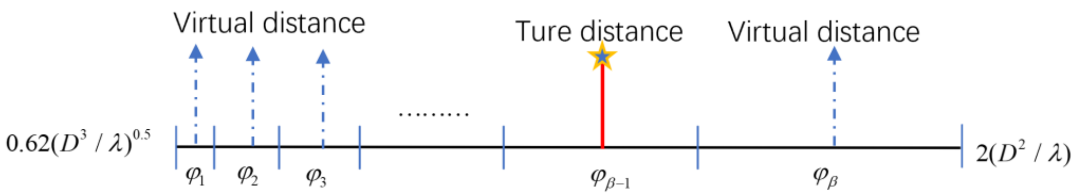


**Figure 3.** Distance information by searching the whole Fresnel region.

There is a certain relationship between these types of distance information, i.e., their reciprocal obeys uniform distribution, and thus, they can be converted by Formula (31). Therefore, we do not need to search spectral peaks in the whole Fresnel region but only in a certain region to obtain the distance information and use the conversion relationship between the distance information to calculate the other distance information using Formula (31).

From Formula (30), we see that the distance of the first subspace is the shortest, so during the simulations, we generally select subspace 1 for the spectral peak search.

In principle, the initial noise subspace matrix $\hat{\boldsymbol{U}}$ is only orthogonal to the guidance vector corresponding to the real position information of the near-field source. Therefore, all distance information is substituted into $\|\hat{\boldsymbol{U}}^H \boldsymbol{a}(\theta_m, r)\|$, and only the real distance information minimizes it. From this principle, the true distance can be found from the $\beta$ distance information:

$$\underset{r}{min}\left\|\hat{\boldsymbol{U}}^H \boldsymbol{a}(\theta_m, r)\right\|. \tag{44}$$

From the above algorithm description, we observe that constructing the intersection $\boldsymbol{U}_{new}$ of the noise subspace clusters is the core problem that the algorithm must solve. Currently, the existing methods solve the multiple subspace intersection using the alternating projection algorithm and the reduced-dimension singular value decomposition method. The above two algorithms are described below.

First, a new matrix $\boldsymbol{P}_k, k = 1, 2, \cdots, \beta$ is constructed using noise subspace clusters $\boldsymbol{U}_k, k = 1, 2, \cdots, \beta$, where $\boldsymbol{P}_k$ is an orthogonal operator of span$(\boldsymbol{U}_k)$, calculated as follows:

$$\boldsymbol{P}_k = \boldsymbol{U}_k(\boldsymbol{U}_k^H \boldsymbol{U}_k)^{-1}\boldsymbol{U}_k^H = \boldsymbol{U}_k \boldsymbol{U}_k^H.. \tag{45}$$

Then, we use $\boldsymbol{P}_k, k = 1, 2, \cdots, \beta$ to define the following matrix $\boldsymbol{Q}$:

$$\boldsymbol{Q} = \beta \boldsymbol{I} - \sum_{k=1}^{\beta} \boldsymbol{P}_k. \tag{46}$$

However, the null space of $\boldsymbol{Q}$ and span$(\boldsymbol{U}_{new})$ is equal, namely:

$$span(\boldsymbol{U}_{new}) = Null(\boldsymbol{Q}). \tag{47}$$

Since span$(\boldsymbol{U}_{new})$ is equal to the null space of $\boldsymbol{Q}$, we obtain the null space of $\boldsymbol{Q}$ by eigenvalue decomposition of $\boldsymbol{Q}$, and then we obtain the new noise subspace cluster required.

We obtain the zero space corresponding to matrix $\boldsymbol{Q}$ by applying matrix decomposition on matrix $\boldsymbol{Q}$. The specific matrix decomposition representation is as follows:

$$\boldsymbol{Q} = \boldsymbol{\Pi}\boldsymbol{\Omega}\boldsymbol{\Xi}^H, \tag{48}$$

where $\boldsymbol{\Pi} = [\Pi_1, \Pi_2, \ldots \Pi_N]$ corresponds to the left singular matrix of matrix $\boldsymbol{Q}$ and $\boldsymbol{\Xi} = [\Xi_1, \Xi_2, \ldots \Xi_N]$ corresponds to the right singular matrix of matrix $\boldsymbol{Q}$.

The above algorithm virtualizes the $L$ near-field sources into the $\beta L$ near-field sources, so we decompose the diagonal matrix $\boldsymbol{\Omega}$ into $\beta L$ large eigenvalues and $N - \beta L$ small eigenvalues. Sorting singular values from largest to smallest provides:

$$\boldsymbol{\tau}_1 \geq \boldsymbol{\tau}_2 \geq \ldots\ldots \geq \boldsymbol{\tau}_{\beta L} > \boldsymbol{\tau}_{\beta L+1} = \ldots\ldots \boldsymbol{\tau}_N = 0. \tag{49}$$

Therefore, Formula (42) can be rewritten as a signal and a noise subspace:

$$\boldsymbol{Q} = \boldsymbol{\Pi}_s \boldsymbol{\Omega}_s {\boldsymbol{\Xi}_s}^H + \boldsymbol{\Pi}_n \boldsymbol{\Omega}_n {\boldsymbol{\Xi}_n}^H, \tag{50}$$

in which:

$$\begin{aligned}
\boldsymbol{\Pi}_s &= [\pi_1, \pi_2, \ldots \pi_{\beta M}], \\
\boldsymbol{\Pi}_n &= [\pi_{\beta M+1}, \pi_{\beta M+2}, \ldots \pi_N], \\
\boldsymbol{\Xi}_s &= [\Xi_1, \Xi_2, \ldots \Xi_{\beta M}], \\
\boldsymbol{\Xi}_n &= [\Xi_{\beta M+1}, \Xi_{\beta M+2}, \ldots \Xi_N].
\end{aligned}$$

From Formula (42), the following formula can be obtained:

$$\boldsymbol{U}_{new} = \left(\Xi_1, \Xi_2, \ldots \Xi_{\beta M}\right) = \Xi_n. \tag{51}$$

Hence, to recap, the proposed algorithm involves the following steps:

1. Construct the special fourth-order cumulative vector $C_{S-IMISC}$ based on the S-IMISC array model;
2. Based on the fourth-order cumulative vector $C_{S-IMISC}$, use Formula (24) to obtain the polynomial coefficients $[\bar{c}_{L-1}, \bar{c}_{L-2}, \cdots, \bar{c}_0]$;
3. Construct a polynomial $f(\chi)$ and obtain the near-field source azimuth information by solving the root of the polynomial;
4. The covariance matrix $\boldsymbol{R}$ is constructed by the data received by forward arrays, as illustrated in Figure 1b. Then, eigenvalue decomposition is performed on the matrix $\boldsymbol{R}$ to obtain the initial noise subspace;
5. Divide the entire Fresnel region into $\beta$ subintervals and construct the corresponding noise subspace $\boldsymbol{U}_k, k = 1, 2, \cdots, \beta$ for each subinterval through Formula (38). Then, construct the intersection of noise subspace clusters $\boldsymbol{Q}$ using Formulas (45) and (46);
6. Obtain the new noise subspace cluster using $\boldsymbol{U}_{new}$ from Formula (51);
7. Construct a spectral function $P_{new}(r)$ and search for the first minimal interval to obtain the distance value $r_1$. Calculate the corresponding distance of other subspaces $r_2, r_3, \ldots\ldots, r_\beta$ through the Formula (32);
8. Select the true distance from the distance value $r_1, r_2, r_3, \ldots\ldots, r_\beta$ using Formula (44).

## 5. Performance Analysis

### *5.1. Analysis of the Uniform DOFs*

This section compares the uniform DOFs of the proposed algorithm against the TSMUSIC algorithm and SDNA. We assume that there are $2N-1$ arrays, the uniform DOFs of the proposed algorithm are $2N(N-1)/3-1$, and the uniform DOFs of the TSMUSIC algorithm are 2N−2. The SDNA algorithm is quite complex and considers two cases. If $N$ is odd, the uniform DOFs are $N^2/2 + N - 0.5$, and if $N$ is even, the uniform DOFs are $N^2/2 + N - 1$. From the above analysis, we conclude that the proposed algorithm has more uniform DOFs than TSMUSIC and SDNA. The uniform DOFs of the proposed algorithm and comparison algorithms is shown in Figure 4.

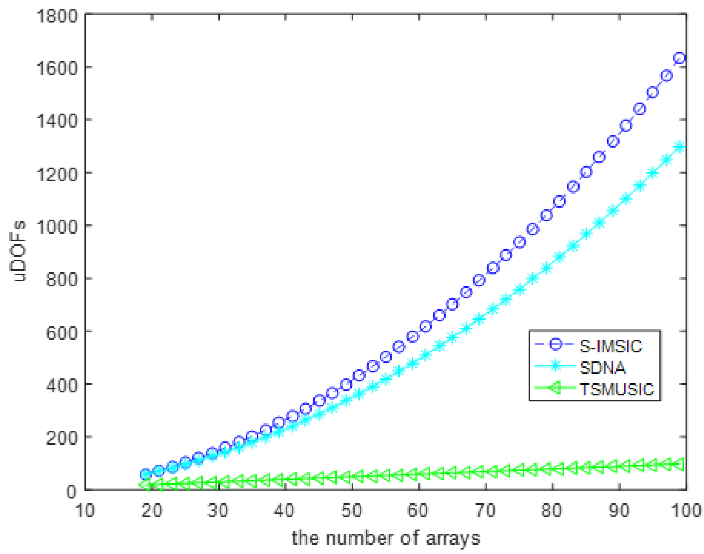


**Figure 4.** uDOFs versus the number of sensors.

*5.2. Computational Complexity*

When analyzing the computational complexity, we only consider the main parts, i.e., multiplications involved in the cumulant matrix construction, EVD implementation, and MUSIC spectral search. The TSMUSIC algorithm and SDNA constructs one $(2N+1)\times(2N+1)$-dimensional and one $(4N+1)\times(4N+1)$-dimensional matrix and implements their EVDs. Meanwhile, the same algorithm requires a one-dimensional MUSIC spectral search applied once on the whole Fresnel area.

The proposed algorithm constructs only one $(2(N-P+3)P-12)$-dimensional and one $(2N-1)\times(2N-1)$-dimensional matrix and one EVD. Moreover, the suggested algorithm searches in the first small area, which is smaller than the whole search area.

From the above theoretical analysis and comparison, our algorithm's computational complexity is lower than the other two.

*5.3. Influence of Mutual Coupling Effect*

This section roughly compares the mutual coupling effects of the S-IMSIC array model and the other two array models using weight functions $\omega(1), \omega(2), \omega(3)$. The latter functions of the S-IMSIC array model are as follows:

$$\omega(1) = 4,\ \omega(2) = \begin{cases} 4\left\lfloor \frac{N+2}{6} \right\rfloor, N \geq 16 \\ 10, 16 > N \geq 10 \end{cases} \quad \omega(3) = \begin{cases} 2, N \geq 16 \\ 4, 16 > N \geq 10 \end{cases}$$

The weight functions $\omega(1), \omega(2), \omega(3)$ of the TS array model are:

$$\omega(1) = 2N-1,\ \ \omega(2) = 2N-2,\ \ \omega(3) = 2N-3,$$

The weight functions $\omega(1), \omega(2), \omega(3)$ of the nested array model are the following:

$$\omega(1) = 2N_1-1,\ \ \omega(2) = 2N_1-2,\ \ \omega(3) = 2N_1-3$$

Comparing the above weight equations highlights that the S-IMSIC has lower $\omega(1), \omega(2), \omega(3)$ values than the other two array models, and therefore, the mutual coupling between the sensors is significantly reduced.

## 6. Numerical Examples

To verify our algorithm's and the S-IMISC's array model performance, we compare them against TOMUSIC, MOMUSIC, and SDNA through Matlab simulation tests. The simulation setup involves 19 array elements, with the placement form illustrated in Figure 1. Three near-field sources are incident, respectively, located at $\{\theta_1 = 20^\circ, r_1 = 3\lambda\}$, $\{\theta_2 = 40^\circ, r_2 = 12\lambda\}$, and $\{\theta_3 = 50^\circ, r_2 = 14\lambda\}$. Meanwhile, we assume that all incident-sources have equal power and the number of sources is known. Through 500 Monte Carlo programs, the corresponding experimental data are obtained. The root mean square error of the experiment result can be presented as:

$$RMSE = \sqrt{\frac{1}{500}\sum_{i=1}^{500}\sum_{j=1}^{K}(\hat{\beta}_j^i - \beta_j)}, \tag{52}$$

In which $\hat{\beta}_j^i$ represents the estimated value of the $j$th near-field source from the $i$th experiment and $\beta_j$ represents the theoretical value of the $j$th near-field source.

The configuration of personal computer used for simulation is as follows: (1) CPU: Intel (R) Core (TM) i7-6500U CPU @ 2.50 GHz; (2) Memory: 8 GB; (3) Hard Drive: 256 GB; (4) Graphics Card: NVIDIA GeForce 940MX, 2 GB, 384 M, 64 bit.

### *6.1. Experiment 1: Angular Parameter Estimation Accuracy*

This section provides numerical examples to illustrate the superiority of the proposed S-IMISC arrays over the existing sparse arrays considering the mutual coupling matrices. These simulations consider the RMSE performance versus the input SNR and the number of snapshots.

Figure 5 depicts the RMSE of the near-field source angle estimates versus the SNR, revealing that the RMSE of the three algorithms decreases as the SNR increases. Moreover, the S-IMSIC array model has a smaller RMSE than the competitor array models. Figure 6 illustrates the RMSE of the near-field source angle estimates versus the number of snapshots, inferring that the RMSE of the three algorithms decreases as the number of snapshots increases. Additionally, the S-IMSIC array model has a smaller RMSE than the competitor models. The S-IMISC array model adopted by the proposed algorithm can thus greatly reduce the effect of the mutual coupling. Meanwhile, the algorithm proposed in this article utilizes the root polynomial method with better parameter estimation performance, which not only reduces computational complexity, but also ensures that accuracy is not affected by the search step size. This further improves estimation accuracy. Therefore, the performance of the S-MISC array model adopted by the proposed algorithm is better than that of the other methods.

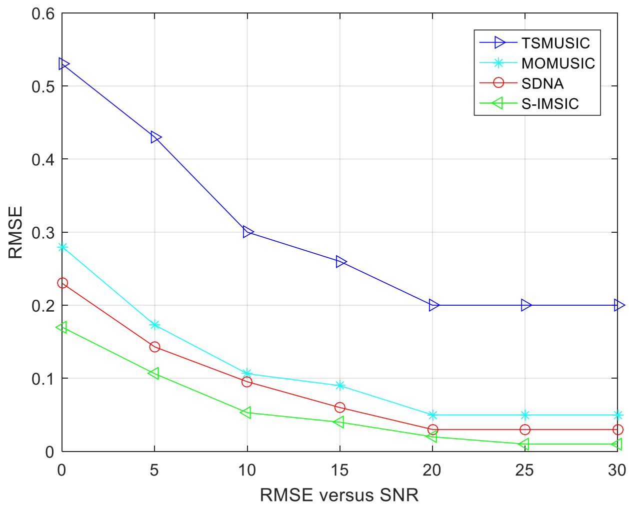


**Figure 5.** RMSE of the azimuth estimates versus SNR (200 snapshots).

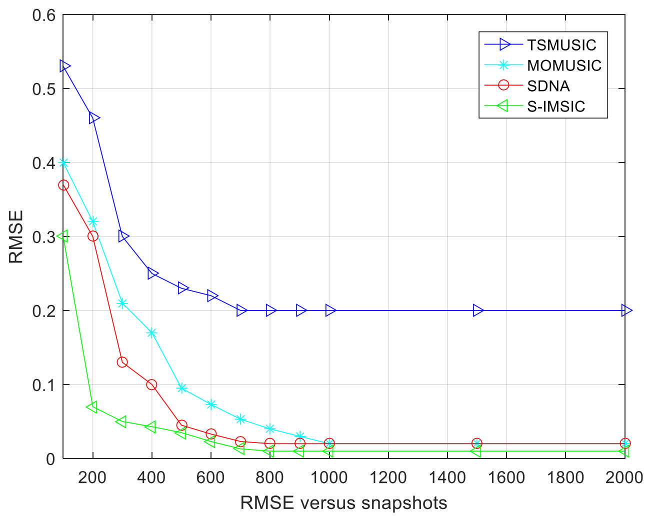


**Figure 6.** RMSE of the azimuth estimates versus the number of snapshots (10 dB SNR).

*6.2. Experiment 2: Distance Parameter Estimation*

In this experiment, the number of subspaces is $\beta = 5$, and we consider the distance search space to be the entire Fresnel distance range. The corresponding simulation results are presented in Figure 7.

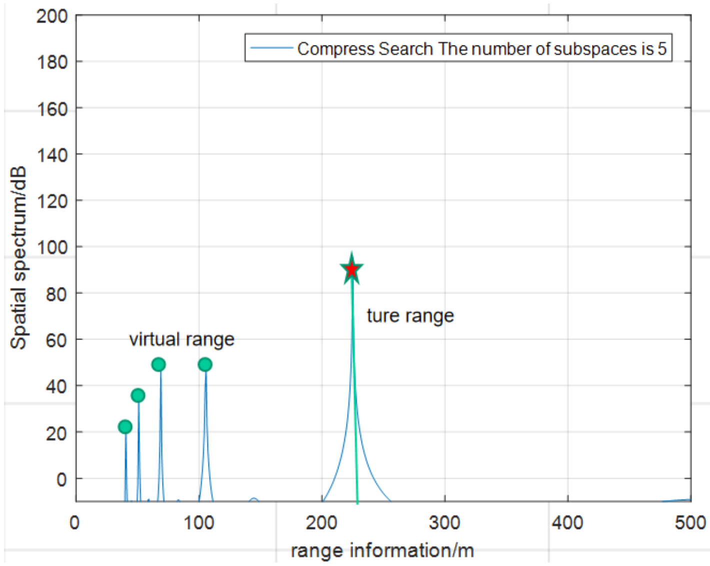


**Figure 7.** Distance information of source 1 obtained by the compression ideal.

Figure 7 reveals that the reasoning results are the same as in the previous section, i.e., there is a spectral peak in the corresponding distance region and only one true distance parameter among the spectral peaks. Therefore, in practical applications, we only search for the first minimum distance interval to obtain distance information, then we use Formula (32) to convert to obtain other distance information in the transformed domain, and finally, we use Formula (44) to find the true distance information.

Since the angular estimation accuracy directly affects the distance parameter estimation accuracy and to separately analyze the performance of the distance parameter estimation scheme proposed in this chapter, we introduce Formula (29) for accurate angle information when estimating the distance.

The root mean square error of the distance estimation under different signal-to-noise ratios is statistically analyzed. The number of snapshots is fixed at 100, the number of distance slices is 2, and the signal-to-noise ratio ranges from 0 dB to 30 dB with an interval of 5 dB. Two hundred Monte Carlo experiments are conducted for each signal-to-noise ratio condition to obtain the estimated root mean square distance error for the two algorithms under different signal-to-noise ratios. The statistical results are illustrated in Figure 8.

Figure 8 highlights that the distance estimation accuracy of the two algorithms improves as SNR increases. However, under the same SNR, the proposed algorithm has a slightly lower distance estimation accuracy than the TS-MUSIC algorithm. Furthermore, under the same SNR conditions, our method's RMSE increases as the number of distance slices increases because the corresponding number of noise subspace clusters increases, and the intersection dimension of the constructed noise subspace clusters decreases. In other words, as the number of noise subspace clusters increases, their intersection reduces, and thus, the information available for spectral peak searching is reduced. Therefore, our algorithm's RMSE increases as distance slices increase.

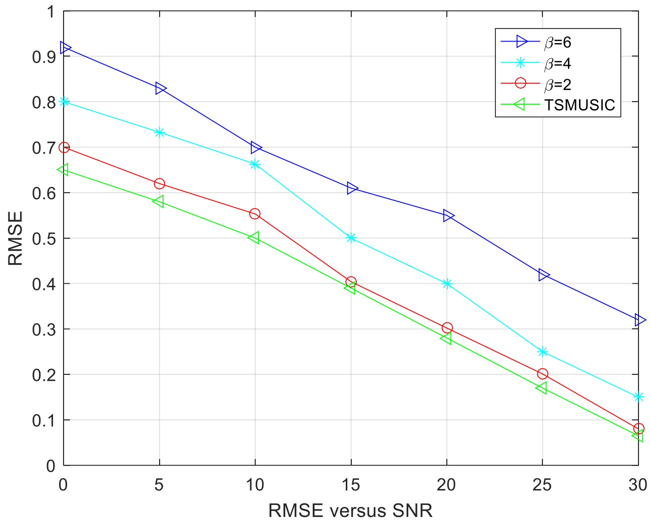


**Figure 8.** The relationship between RMSE values of range and SNR.

### 6.3. Experiment 3: Computation Time Comparison

Next, we use MATLAB to verify the computational complexity of the proposed algorithm. When estimating distance parameters, the algorithm divides the subspace $\beta$ into two and five. Each point is subjected to 500 Monte Carlo experiments, and the calculation time of the two algorithms is statistically averaged. The results are reported in Table 1.

**Table 1.** Computation time (s).

| Methods | | Computation Time (s) |
|---|---|---|
| TS-MUSIC algorithm | | 2.84122 |
| SDNA | | 2.55455 |
| MOMUSIC algorithm | | 3.25872 |
| The proposed algorithm | $\beta = 2$ | 1.22276 |
| | $\beta = 5$ | 1.03323 |

Table 1 highlights that the processing time of the developed algorithm is much less than that of the competitor algorithms because our algorithm exploits the seeking roots method to replace the eigenvalue decomposition and spectral peak search processes that MOMUSIC, TSMUSIC and SDNA use for the angular estimation. This strategy reduces our algorithm's computational complexity. Moreover, for the distance estimation, a small search area replaces searching the entire Fresnel region, further reducing the computational complexity. Additionally, Table 1 reveals that the simulation time of the algorithm decreases as the search area increases. Indeed, the more the distance slices $\beta$, the smaller the area to search and the smaller the simulation time. This simulation experiment demonstrates that the proposed algorithm significantly reduces the computational complexity and processing time.

## 7. Conclusions

This paper proposes a novel array model named S-IMISC for near-field sources location. The S-IMISC array model has all the advantages of the nested array models. In the case of a certain number of arrays, the positioning of the S-IMISC array can be uniquely determined by a closed formula. Meanwhile, the S-IMISC array model has more uDOFs and fewer mutual compiling effects than current sparse array models with the same number of arrays. Additionally, in order to improve positioning speed, we develop an ideal of CEM for the azimuth estimation of near-field sources, and compression is used to reduce the range research, significantly reducing the computational complexity. Extensive simulations verify the several advantages of the S-IMISC array models and the proposed algorithm, namely, more uDOFs, fewer mutual compiling effects, and lower computational complexity.

**Author Contributions:** Conceptualization, X.L.; methodology, X.L.; software, H.Y.; validation, X.L., H.Y. and J.H.; formal analysis, N.D.; investigation, N.D.; resources, X.L.; data curation, X.L.; writing—original draft preparation, X.L.; writing—review and editing, H.Y. and J.H. All authors have read and agreed to the published version of the manuscript.

**Funding:** This research was funded by project ZR2019BF046 supported by Shandong Provincial Natural Science Foundation and Yantai Science and Technology Innovation Program (2022JMRH003).

**Data Availability Statement:** The data presented in this study are available on request from the corresponding author.

**Conflicts of Interest:** The authors declare no conflict of interest.

## References

1. Li, F.; Liu, H. Statistical analysis of beam-space estimation for direction-of-arrivals. *IEEE Trans. Signal Process.* **1994**, *42*, 604–610.
2. Zhuang, J.; Li, W.; Manikas, A. Fast root-MUSIC for arbitrary arrays. *Electron. Lett.* **2010**, *46*, 174–176. [CrossRef]
3. Wu, J.; Wang, T.; Bao, Z. Fast realization of root MUSIC using multi-taper real polynomial rooting. *Signal Process.* **2015**, *106*, 55–61. [CrossRef]
4. Starer, D.; Nehorai, A. Passive localization of near-field sources by path following. *IEEE Trans. Signal Process.* **1994**, *42*, 677–680. [CrossRef]
5. He, J.; Swamy, M.N.S.; Ahmad, M.O. Efficient Application of MUSIC Algorithm Under the Coexistence of Far-Field and Near-Field Sources. *IEEE Trans. Signal Process.* **2012**, *60*, 2066–2070. [CrossRef]
6. Liang, J.; Yang, S.; Zhang, J. A New Near-Field Source Localization Algorithm without Pairing Parameters. In Proceedings of the Fourth IEEE Workshop on Sensor Array and Multichannel Processing, Waltham, MA, USA, 12–14 July 2006; pp. 162–165.
7. Wu, Y.; So, H.C.; Hou, C.; Li, J. Passive Localization of Near-Field Sources with a Polarization Sensitive Array. *IEEE Trans. Antennas Propag.* **2007**, *55*, 2402–2408. [CrossRef]
8. Weiss, A.; Friedlander, B. Range and bearing estimation using polynomial rooting. *IEEE J. Ocean. Eng.* **1993**, *18*, 130–137. [CrossRef]
9. Liang, J.; Liu, D. Passive Localization of Mixed Near-Field and Far-Field Sources Using Two-stage MUSIC Algorithm. *IEEE Trans. Signal Process.* **2009**, *58*, 108–120. [CrossRef]
10. Molaei, A.M.; Zakeri, B.; Andargoli, S.M.H. A one-step algorithm for mixed far-field and near-field sources localization. *Digit. Signal Process.* **2021**, *108*, 102899. [CrossRef]
11. Chen, J.; Hudson, R.; Yao, K. Maximum-likelihood source localization and unknown sensor location estimation for wideband signals in the near-field. *IEEE Trans. Signal Process.* **2002**, *50*, 1843–1854. [CrossRef]
12. Jianzhong, L.; Wang, Y.; Gang, W. Signal reconstruction for near-field source localisation. *IET Signal Process.* **2015**, *9*, 201–205. [CrossRef]
13. Wang, B.; Liu, J.; Sun, X. Mixed Sources Localization Based on Sparse Signal Reconstruction. *IEEE Signal Process. Lett.* **2012**, *19*, 487–490. [CrossRef]
14. Zhi, W.; Chia, M.Y.-W. Near-field source localization via symmetric subarrays. *IEEE Signal Process. Lett.* **2007**, *14*, 409–412. [CrossRef]
15. Pal, P.; Vaidyanathan, P.P. Nested Arrays: A Novel Approach to Array Processing with Enhanced Degrees of Freedom. *IEEE Trans. Signal Process.* **2010**, *58*, 4167–4181. [CrossRef]
16. Liu, C.-L.; Vaidyanathan, P.P. Super Nested Arrays: Linear Sparse Arrays with Reduced Mutual Coupling—Part I: Fundamentals. *IEEE Trans. Signal Process.* **2016**, *64*, 3997–4012. [CrossRef]
17. Ren, S.; Dong, W.; Li, X.; Wang, W.; Li, X. Extended Nested Arrays for Consecutive Virtual Aperture Enhancement. *IEEE Signal Process. Lett.* **2020**, *27*, 575–579. [CrossRef]
18. Liu, J.; Zhang, Y.; Lu, Y.; Ren, S.; Cao, S. Augmented Nested Arrays with Enhanced DOF and Reduced Mutual Coupling. *IEEE Trans. Signal Process.* **2017**, *65*, 5549–5563. [CrossRef]
19. Yang, M.; Sun, L.; Yuan, X.; Chen, B. Improved nested array with hole-free DCA and more degrees of freedom. *Electron. Lett.* **2016**, *52*, 2068–2070. [CrossRef]
20. Pal, P.; Vaidyanathan, P.P. Coprime sampling and the MUSIC algorithm. In Proceedings of the 2011 Digital Signal Processing and Signal Processing Education Meeting (DSP/SPE), Sedona, AZ, USA, 4–7 January 2011; pp. 289–294.
21. Wang, X.; Yang, Z.; Huang, J.; de Lamare, R.C. Robust Two-Stage Reduced-Dimension Sparsity-Aware STAP for Airborne Radar with Coprime Arrays. *IEEE Trans. Signal Process.* **2020**, *68*, 81–96. [CrossRef]
22. Vaidyanathan, P.P.; Pal, P. Sparse Sensing with Co-Prime Samplers and Arrays. *IEEE Trans. Signal Process.* **2011**, *59*, 573–586. [CrossRef]

23. Vaidyanathan, P.; Pal, P. Sparse sensing with coprime arrays. In Proceedings of the 2010 Conference Record of the Forty Fourth Asilomar Conference on Signals, Systems and Computers, Pacific Grove, CA, USA, 7–10 November 2010; pp. 1405–1409.
24. Zheng, Z.; Wang, W.-Q.; Kong, Y.; Zhang, Y.D. MISC Array: A New Sparse Array Design Achieving Increased Degrees of Freedom and Reduced Mutual Coupling Effect. *IEEE Trans. Signal Process.* **2019**, *67*, 1728–1741. [CrossRef]
25. Shi, W.; Li, Y.; de Lamare, R.C. Novel Sparse Array Design Based on the Maximum Inter-Element Spacing Criterion. *IEEE Signal Process. Lett.* **2022**, *29*, 1754–1758. [CrossRef]
26. Wang, B.; Zhao, Y.; Liu, J. Mixed-Order MUSIC Algorithm for Localization of Far-Field and Near-Field Sources. *IEEE Signal Process. Lett.* **2013**, *20*, 311–314. [CrossRef]
27. Zheng, Z.; Fu, M.; Wang, W.-Q.; Zhang, S.; Liao, Y. Localization of Mixed Near-Field and Far-Field Sources Using Symmetric Double-Nested Arrays. *IEEE Trans. Antennas Propag.* **2019**, *67*, 7059–7070. [CrossRef]
28. Su, X.; Hu, P.; Gong, Z.; Liu, Z.; Shi, J.; Li, X. Convolution Neural Networks for Localization of Near-Field Sources via Symmetric Double-Nested Array. *Wirel. Commun. Mob. Comput.* **2021**, *2021*, 9996780. [CrossRef]
29. Wang, Y.; Cui, W.; Du, Y.; Ba, B.; Mei, F. A Novel Sparse Array for Localization of Mixed Near-Field and Far-Field Sources. *Int. J. Antennas Propag.* **2021**, *2021*, 3960361. [CrossRef]
30. Wang, Y.; Cui, W.; Yang, B.; Ba, B.; Mei, F. Symmetric thinned coprime array with reduced mutual coupling for mixed near-field and far-field sources localization. *IET Radar Sonar Navig.* **2022**, *16*, 1292–1303. [CrossRef]
31. Wang, Y.; Cui, W.; Ba, B.; Du, B.; Yang, Y. Improved symmetric flipped nested array for mixed near-field and far-field non-circular sources localization. *IET Commun.* **2023**, *17*, 737–746. [CrossRef]
32. Liu, Z.-M.; Huang, Z.-T.; Zhou, Y.-Y. Computationally efficient direction finding using uniform linear arrays. *IET Radar Sonar Navig.* **2012**, *6*, 39–48. [CrossRef]
33. Yan, F.; Jin, M.; Qiao, X. Low-Complexity DOA Estimation Based on Compressed MUSIC and Its Performance Analysis. *IEEE Trans. Signal Process.* **2013**, *61*, 1915–1930. [CrossRef]